Available online at www.sciencedirect.com
ScienceDirect
Scripta Materialia 59 (2008) 912–915
Scripta MATERIALIA
www.elsevier.com/locate/scriptamat

Viewpoint Paper

Surface oxide effects on failure of polysilicon MEMS after cyclic and monotonic loading

H. Kahn,[a,*] A. Avishai,[a] R. Ballarini[b] and A.H. Heuer[a]

[a] *Department of Materials Science and Engineering, Case Western Reserve University, 10900 Euclid Ave, Cleveland, OH 44106, United States*

[b] *Department of Civil Engineering, University of Minnesota, Minneapolis, MN 55455, United States*

Received 16 November 2007; accepted 14 December 2007
Available online 14 January 2008

Abstract—Polycrystalline silicon (polysilicon) microelectromechanical systems (MEMS) devices subjected to constant tensile stresses do not display delayed fracture in humid ambients unless they also contain thick (>45 nm) surface oxide layers, which are then susceptible to moisture-assisted stress corrosion. Polysilicon MEMS devices with typical (~3 nm thick) native oxides do not show any thickening of the surface oxide layer after 3×10^7 fatigue cycles, excluding stress corrosion of the surface oxide as a cause of fatigue failure. Possible origins of polysilicon fatigue are discussed.

Keywords: Microelectromechanical systems (MEMS); Fatigue fracture; High-resolution electron microscopy (HREM)

The existence of fatigue in polycrystalline silicon (polysilicon) microelectromechanical systems (MEMS) devices has been well established, but its origin has been a matter of debate. As described in two recent reviews [1,2], the two main explanations involve mechanical and environmental effects. Supporting the mechanical damage mechanism are experimental results that show: (i) a strong dependence of fatigue strength on the load ratio R (the ratio of the lowest stress to highest stress in the fatigue cycle), but no dependence on the testing environment using either air or low vacuum (10 Pa) [3]; (ii) no dependence on the frequency of the cyclic load – in other words, a dependence on the number of stress cycles but not on time [4]; (iii) an actual increase in the strength of the devices after certain cyclic stress conditions [5,6]; (iv) no extension of sharp pre-cracks held under constant high tension in humid air environments [3]; and (v) observed polysilicon fatigue in vacuum (though at much longer times than for air tests) [6]. Also, recent results for bulk single crystal silicon demonstrate decreased strength after cyclic compressive loading but not after constant loading, which is attributed to mechanical damage accumulation [7].

The main drawback to the mechanical explanation for polysilicon fatigue is that no specific physical mechanisms have been suggested that can explain all the observed fatigue behavior. Recent molecular dynamics simulations of nanocrystalline silicon have demonstrated that plasticity can occur in grain boundary regions [8]. Incorporating this effect into a finite element model of polysilicon led to a proposed strengthening model [5] in which cyclic loads generate residual compressive stresses at the notch root, which in turn result in an apparent increase in tensile strength upon subsequent loading. The molecular dynamics simulations [8] also suggest that if the applied stresses are high enough, microcracks and voids could develop that would decrease strength. This has not yet been incorporated into a finite element model with applied cyclic stresses. However, this analysis cannot explain fatigue observed for single crystal silicon devices [9].

The environmental explanation for polysilicon fatigue describes a degradation process involving subcritical cracking within the thickening silicon dioxide layer on the surface of the devices. This cyclic stress-induced thickening of this oxide reaction layer leads to continued crack growth until a critical length is reached (“reaction layer fatigue” [10]). Stress corrosion cracking of bulk silicon dioxide due to humidity is well documented. The strongest evidence in support of this mechanism is the

* Corresponding author. Tel.: +1 216 368 6384; e-mail: kahn@case.edu

1359-6462/$ - see front matter © 2008 Acta Materialia Inc. Published by Elsevier Ltd. All rights reserved.
doi:10.1016/j.scriptamat.2007.12.025

extended fatigue lifetimes seen in vacuum and other low humidity environments for both polysilicon [3,6,11] and single crystal silicon [9,12]. In addition, transmission electron microscopy (TEM) investigations have reported thicker surface oxides in the areas of the devices that experienced highest cyclic stresses [10,11]. The earlier study was complicated by an anomalously thick surface oxide (~30 nm) on the devices before test [10], but the effect was recently confirmed for polysilicon devices with more typical air-formed oxide thicknesses (~3 nm) [11]. Besides a lack of explanation for some of the observed fatigue behavior just discussed, one drawback of the environmental model is that fatigue failures are routinely seen at $<10^6$ cycles, which is <30 s for these devices [10,11], and it is difficult to imagine a room temperature oxidation process that would thicken the surface oxides so rapidly.

In this letter, we describe our TEM investigations on polysilicon surface oxides after fatigue testing. We also report the effects of oxide thickness on delayed fracture of polysilicon under constant tensile stress. We have previously demonstrated that polysilicon beams with sharp pre-cracks do not display crack extension under constant tensile stress in humid air [3]. In addition, we have fabricated a series of clamped–clamped beams from a 2 μm thick low-pressure chemical-vapor deposited (LPCVD) polysilicon film using standard surface-micromachining techniques, shown in Figure 1. The undoped polysilicon was deposited at 570 °C and annealed at 615 °C to produce a fine-grained (~0.1 μm), equiaxed microstructure with a tensile residual stress of 318 MPa, as determined by rotating microstrain gauges. The beams are 500 μm long and 20 μm wide, and each beam contains a micromachined notch with root radius of 0.9 μm but of varying depth. The notch depths were measured using scanning electron microscopy (SEM). The resulting stress concentrations at the notch root due to the residual tensile stress were then determined using finite element analysis (FEA). After release, for enhanced stresses greater than the fracture strength, catastrophic failure ensued, as seen in the lower inset in Figure 1. From the FEA, the fracture strength was 3.9 GPa. The surviving beams (from 14 total devices) were placed in a chamber containing room temperature air at 90% relative humidity. After 3000 h, no additional beams broke even though the stresses in some of the beams must have been extremely close to the fracture strength. This essentially confirms the absence of stress corrosion in notched polysilicon specimens subjected to constant loads.

After release, our polysilicon devices exhibited surface oxides with thicknesses of ~3 nm, as determined by X-ray photoelectron spectroscopy, typical of "native oxide" growth on silicon surfaces in air. To investigate the effects of thicker surface oxides, devices usually used for fatigue testing [3,5], shown in Figure 2, were used. Since compressive stresses are generated during polysilicon oxidation [13], the devices in Figure 1 were not suitable. However, the devices in Figure 2 contained large comb-drive actuators which could be pushed downward and then adhered to the substrate using drops of water, creating constant tensile stresses at the notch roots of the specimens shown in the inset to Figure 2. The 6 μm thick specimens were deflected to achieve a tensile stress of ~3.2 GPa at the notch root, as determined by FEA, ignoring any local stresses created by oxidation. For each oxide thickness to be studied, 4–6 polysilicon devices were oxidized in air at 920 °C to achieve oxide thicknesses of 45, 70, 82 and 140 nm, as measured by spectrophotometry on the single crystal silicon substrates. After 200 h in 90% relative humidity air, approximately half of all the specimens had broken. Presumably, moisture-assisted stress corrosion of the surface thermal oxide resulted in crack initiation and growth within the oxide layer, sufficient to cause catastrophic crack propagation through the polysilicon specimen. Using the standard relation for fracture toughness $K_{Ic} = k\sigma_{crit}(\pi a)^{1/2}$, where σ_{crit} is the stress at failure, a is the size of the crack-initiating flaw, and k is a constant equal to 0.71 for a semi-circular flaw [14], and using $K_{Ic} = 1.0\ \mathrm{MPa{\cdot}m^{1/2}}$ [15], the critical flaw size is ~60 nm. This is roughly consistent with the oxide thicknesses used here.

To investigate cyclic stress-induced oxidation, a device like that shown in Figure 2 was fatigued using a stress range of 5.4 GPa, with a maximum stress of 3.6 GPa and a mean stress of 0.9 GPa, at 7.6 kHz, until the specimen fractured after 2×10^7 cycles. The area of the notch adjacent to the fracture was cut out and thinned using focused ion beam (FIB) machining and viewed using TEM. The TEM specimen preparation is illustrated in Figure 3. Briefly, the portion of the device below the fatigue fracture (Fig. 3a) was broken off using

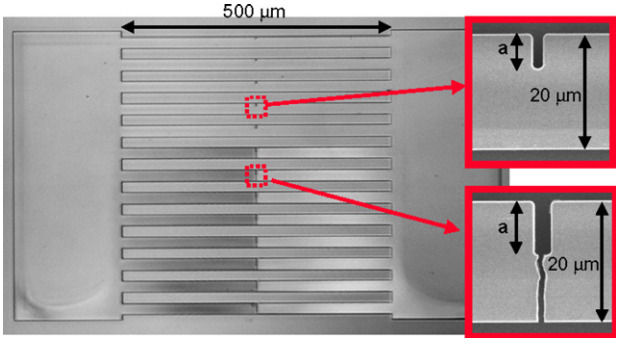

Figure 1. Optical micrograph of a clamped–clamped beam polysilicon device used to study fracture strength and static fatigue. Each of the 13 beams is fixed on both ends and contains a notch of depth, a. The insets are higher magnification SEM images showing two of the 13 notches after release.

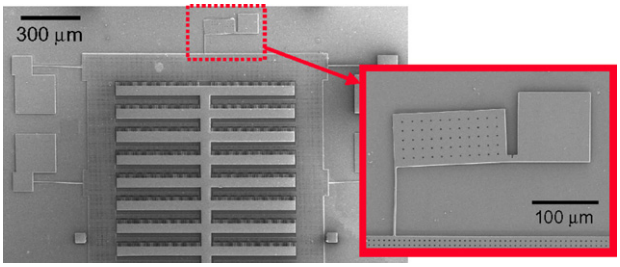

Figure 2. SEM image of an oxidized polysilicon device, deflected such that the maximum stress at the notch root is 90% of the average monotonic strength. The inset shows a higher magnification view of the specimen, showing the notch.

a micromanipulator. To avoid possible ion beam amorphization of the surface of interest, an initial thin electron beam-deposited Pt layer was deposited on the notch root. Then a side trench was FIB-cut to form a beam-like structure (Fig. 3b). Material behind the fracture site was thinned by FIB milling (Fig. 3c). As the polysilicon behind the fracture was milled further, the non-thinned region fortuitously began to tilt upward (Fig. 3d). (This type of FIB milling-induced tilting/artifact was previously reported and utilized for single crystal silicon [16].) Further milling caused tilting to the full perpendicular orientation, and the fracture surface and notch root were protected with a thick ion beam-deposited Pt layer (Fig. 3e). The tilted polysilicon piece was FIB-cut free from the rest of the device and transferred to a TEM grid, where it was attached with ion beam-deposited Pt (Fig. 3f). It was then thinned further in the FIB to become electron-transparent.

A low magnification bright field TEM image taken in a high-resolution TEM is presented in Figure 4a, and high-resolution TEM images of the three locations noted in Figure 4a are shown in Figure 4b–d. In all three areas – the area away from the notch root that experienced very low applied cyclic stress (Fig. 4b), the area at the notch root next to the fracture which experienced the highest cyclic stresses (Fig. 4c) and the area of the fracture surface that experienced no applied stresses (Fig. 4d) – the surface oxide is seen as a bright amorphous layer on top of the crystalline polysilicon. Its

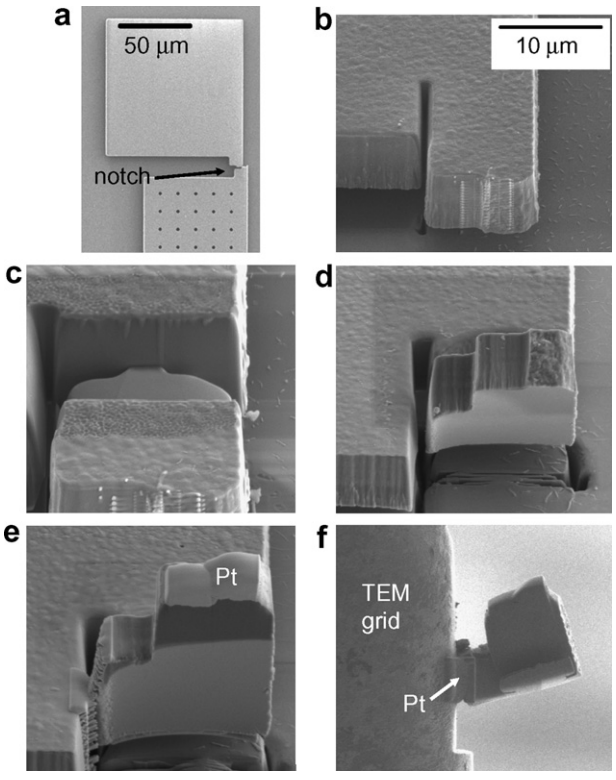

Figure 3. SEM images showing TEM sample preparation of a polysilicon MEMS device near the fatigue fracture. (a) The device showing fatigue fracture at the notch root. (b–e) Tilting and removal of the portion of the device adjacent to the fatigue fracture using FIB machining. (f) The removed portion of the device attached to a TEM grid. See text for more details.

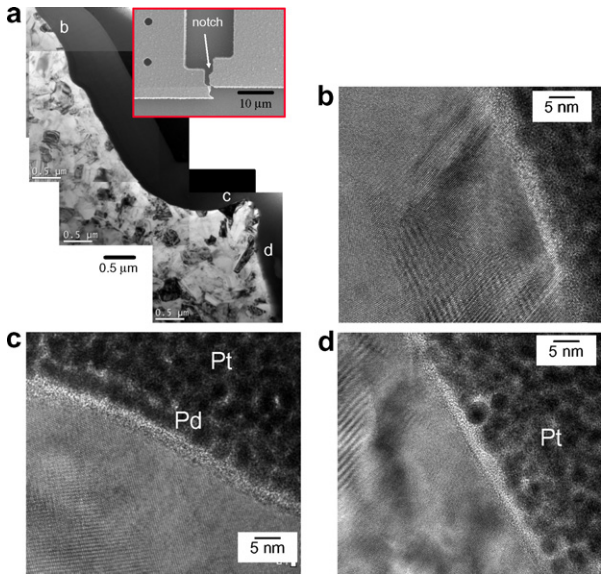

Figure 4. (a) Low magnification TEM image of the notch root region of a polysilicon fatigue specimen after fracture (3×10^7 cycles), shown in the SEM image in the inset. (b–d) High-resolution TEM images of the three areas noted in (a), (b) away from the notch root, (c) at the notch root, and (d) along the fracture surface.

thickness is a constant ~3 nm. This thickness of the surface oxide was confirmed by X-ray energy dispersive spectroscopy (XEDS) line scans in the TEM. Clearly, no oxide growth occurred due to the high cyclic stresses.

The same TEM investigation was repeated with a fracture specimen that failed after 6×10^6 cycles under the same stress conditions. High-resolution TEM images of the high stress area at the notch root and the newly formed fracture surface are shown in Figure 5a and b, respectively. The observed oxide layers are essentially indistinguishable from those in Figure 4. In Figure 4b–d and Figure 5a and b, the contrast seen beyond the oxide layer is due to Pt deposited during FIB machining. In Figure 4c and Figure 5a, a separate layer next to the oxide can be seen which corresponds to the thin Pd layer that was sputtered onto the devices before fatigue testing, to ensure sufficient electrical conductivity for the electrostatic actuation [3].

Although the LPCVD polysilicon material and fatigue stress conditions for the devices shown in Figures 4 and 5 were very similar to those reported by Alsem et al. [10], they observed oxide thickening at the notch

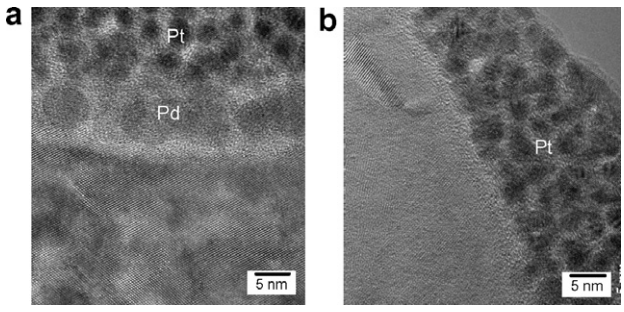

Figure 5. High-resolution TEM images of a polysilicon fatigue specimen after fracture (6×10^6 cycles): (a) at the notch root and (b) along the fracture surface.

root, and we do not. Our experiments on notched polysilicon devices subjected to constant tensile stresses demonstrate that these structures are susceptible to delayed fracture only if they contain relatively thick (>45 nm) surface oxides. If oxides on this order can form during room temperature cyclic loading ("reaction layer fatigue"), this can certainly explain much of the observed silicon fatigue behavior. However, we do not detect such cyclic loading-induced oxide thickening in our devices.

The mechanism(s) responsible for silicon fatigue will remain a disputed topic until a comprehensive explanation is developed. The observed phenomena of cyclic stress-induced strengthening and fatigue strength dependence on load ratio R strongly suggest a mechanical root cause. Whether the obvious environmental effect of extended fatigue lifetimes in low humidity and vacuum ambients represents a modification of the mechanical origin or a completely different mechanism is still not known. It would be satisfying if a single class of fatigue mechanisms could be elucidated that was independent of specimen processing conditions.

We thank Hendrik Colijn of the Ohio State University for assistance with the XEDS analysis. Portions of this work were supported by the U.S. Defense Advanced Research Projects Agency.

References

[1] H. Kahn, R. Ballarini, A.H. Heuer, Current Opinion in Solid State and Materials Science 8 (2004) 71–76.
[2] D.H. Alsem, O.N. Pierron, E.A. Stach, C.L. Muhlstein, R.O. Ritchie, Advanced Engineering Materials 9 (2007) 15–30.
[3] H. Kahn, R. Ballarini, J.J. Bellante, A.H. Heuer, Science 298 (2002) 1215–1218.
[4] J. Bagdahn, W.N. Sharpe Jr., Sensors and Actuators A 103 (2003) 9–15.
[5] H. Kahn, L. Chen, R. Ballarini, A.H. Heuer, Acta Materialia 54 (2006) 667–678.
[6] R.E. Boroch, R. Mueller-Fiedler, J. Bagdahn, P. Gumbsch, Scripta Materialia 59 (2008) 936–940.
[7] S. Bhowmick, J.J. Melendez-Martinez, B.R. Lawn, Applied Physics Letters 91 (2007).
[8] M.J. Demkowicz, A.S. Argon, D. Farkas, M. Frary, Philosophical Magazine 87 (2007) 4253–4271.
[9] O.N. Pierron, C.L. Muhlstein, Journal of Microelectromechanical Systems 15 (2006) 111–119.
[10] C.L. Muhlstein, E.A. Stach, R.O. Ritchie, Acta Materialia 50 (2002) 3579–3595.
[11] D.H. Alsem, R. Timmerman, B.L. Boyce, E.A. Stach, J.Th.M. De Hosson, R.O. Ritchie, Journal of Applied Physics 101 (2007) 013515-1–013515-9.
[12] T. Tsuchiya, A. Inoue, J. Sakata, M. Hashimoto, A. Yokoyame, M. Sugimoto, in: Technical Digest of the Sensor Symposium, vol. 16, 2–3 June 1998, Kawasaki, Japan, Tokyo, Institute of Electrical Engineers of Japan, 1998, pp. 277–280.
[13] H. Kahn, N. Jing, M. Huh, A.H. Heuer, Journal of Materials Research 21 (2006) 209–214.
[14] I.S. Raju, J.C. Newman Jr., Engineering Fracture Mechanics 11 (1979) 817–829.
[15] R. Ballarini, H. Kahn, N. Tayebi, A.H. Heuer, Mechanical Properties of Structural Films, ASTM STP 1413 (2001) 37–51.
[16] N. Wang, Microscopy Today 13 (2005) 36–39.